An Efficient Method of Passive Emitter Location

KLAUS BECKER
Forschungsinstitut fuer Funk und Mathematik

As is well known, the position of a stationary emitter can be estimated by a single moving sensor from passive measurements taken at different points along the trajectory. Usually the position is estimated from bearing measurements. Other measurement sets define alternative locating procedures. One alternative is based on the measurements of the Dopplerized radiated frequency. It is shown that the location methods based on bearing or frequency measurements differ significantly. The characteristic features of each method clearly come to light by investigating the impact of single measurements on the Cramer Rao bound. The substantial differences between both methods lead to a significant integration gain when the combined set of bearing and frequency measurements is processed. The theoretical conclusions are confirmed in a Monte-Carlo computer simulation.

Manuscript received June 28, 1991; revised November 8, 1991.

IEEE Log No. 9202246.

Author's address: Forschungsinstitut für Funk und Mathematik, Abteilung SuS, Neuenahrer Strasse 20, D-5307 Wachtberg-Werthhoven, Germany.

I. INTRODUCTION

The problem of locating a stationary emitter from passive measurements is encountered in a variety of radar and sonar applications. The location can be performed either in an array of spatially distributed sensors or by a single sensor. As opposed to an array, an individual sensor, however, can extract information on the emitter position from its own movement only, i.e., from measurements taken asynchronously along its trajectory.

Passive position location by a single moving sensor offers in some cases advantages compared with other systems. For instance, the individual sensor, due to its autonomy, is able to carry out a mission independently. This can be used in different ways by the various applications. Reconnaissance alone as well as missile control aspects can be of major interest here.

A position estimate can principally be derived from a measurement set of any physical quantity which in the absence of noise and interference uniquely defines the emitter position. This provides some alternative locating procedures.

The standard method is based on bearing measurements at different points along the sensor trajectory. This method is called the bearing method (BM) and has been the topic of much research in the past [1–10]. The investigations performed include sensor location uncertainties [6, 7] and systematic measurement errors as well [8–10].

Another method is based on the Doppler shift of the emitter frequency due to the relative motion between the sensor and the emitter. Since the Doppler shift is a function of the sensor-emitter motion, it can be exploited for emitter state estimation, if the sensor motion is known [3, 11]. Thus, the position of a stationary emitter can be estimated from several frequency measurements taken at different points in the sensor trajectory. If the transmitted frequency is unknown, it has to be treated as an additional state variable. This method is called the frequency method (FM) in the sequel.

Apparently, the combined set of bearing and frequency measurements can also be exploited for emitter position estimation. In doing so, another locating procedure, the so-called combined method (CM), results.

The main contribution of this study is a comparison of the less usual location methods FM and CM with each other and with conventional BM. It turns out that CM is a very powerful method of passive emitter location. Its properties become understandable only from the behavior of its components BM and FM. An intuitive understanding and a deeper insight into BM and FM can be gained by investigating the influence of single measurements on the estimation accuracy within the framework of a Cramer Rao (CR) analysis. This is another important result of this study. The conclusions

from the theoretical CR analysis are confirmed in a numerical simulation taking the maximum likelihood (ML) estimation as estimation procedure.

II. MATHEMATICAL MODEL

For a demonstration of the benefits from simultaneously processing bearing and frequency measurements, the three-dimensional location problem is not particularly more enlightening than the two-dimensional one. Thus, for computational ease the investigations are restricted to the special case where the emitter and the sensor trajectory lie in a plane.

Consider a stationary emitter with coordinates (x_e,y_e) and a sensor moving with velocity v in a plane. At the points (x_i,y_i) the sensor is taking bearing and/or frequency measurements in order to estimate the position of the emitter (Fig. 1). Now, let γ_i denote the true (noise free) bearing to the emitter relative to the velocity of the sensor $\mathbf{v}_i = (\dot{x}_i,\dot{y}_i)$ and let ν_i denote the true (Doppler-shifted but noise free) signal frequency at the ith measurement point along the sensor trajectory. If c is the signal velocity and ν_0 (assumed constant) the transmitted frequency, then line-of-sight (LOS) propagation implies that

$$\gamma_i = \cos^{-1}\left[\frac{\mathbf{v}_i\cdot(\mathbf{r}_e-\mathbf{r}_i)}{|\mathbf{v}_i||\mathbf{r}_e-\mathbf{r}_i|}\right] = \cos^{-1}\left[\frac{\dot{x}_i(x_e-x_i)+\dot{y}_i(y_e-y_i)}{\sqrt{\dot{x}_i^2+\dot{y}_i^2}\sqrt{(x_e-x_i)^2+(y_e-y_i)^2}}\right] \tag{1}$$

and

$$\nu_i = \nu_0 + \frac{\nu_0}{c}\frac{\mathbf{v}_i\cdot(\mathbf{r}_e-\mathbf{r}_i)}{|\mathbf{r}_e-\mathbf{r}_i|} = \nu_0 + \frac{\nu_0}{c}\frac{\dot{x}_i(x_e-x_i)+\dot{y}_i(y_e-y_i)}{\sqrt{(x_e-x_i)^2+(y_e-y_i)^2}}. \tag{2}$$

Throughout, it is assumed that the sensor motion is accurately known. The variables γ_i and ν_i are functions of the emitter coordinates. If the transmitted frequency is unknown, as is supposed in this study, ν_i is a function of ν_0 as well. Hence

$$\gamma_i = \gamma_i(x_e,y_e) \qquad \nu_i = \nu_i(\nu_0,x_e,y_e). \tag{3}$$

In the absence of noise and interference, several bearing or frequency measurements along the sensor trajectory define a single point which is the true emitter position. In the presence of noise, however, BM and FM no longer lead to a single point compatible with all measurements. Consequently, some processing is required, and the location problem becomes a problem of parameter estimation from noisy measurements. From (3) the parameter vector

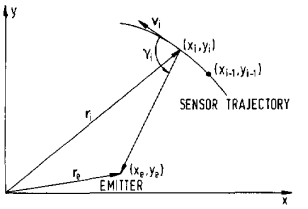

Fig. 1. Two-dimensional sensor-emitter geometry.

to be estimated is $\mathbf{a}_B^T = (x_e,y_e)$ if BM is applied and $\mathbf{a}_F^T = (\nu_0,x_e,y_e)$ if FM is applied.

Let γ_i^m denote the measured bearing and ν_i^m denote the measured frequency, respectively, and let a set of M_B bearing measurements and independent of it a set of M_F frequency measurements be collected at various positions in the sensor trajectory, then in the presence of additive errors

$$\gamma_i^m = \gamma_i(\mathbf{a}_B) + (n_B)_i, \qquad i = 1,\ldots,M_B \tag{4}$$

and

$$\nu_i^m = \nu_i(\mathbf{a}_F) + (n_F)_i, \qquad i = 1,\ldots,M_F \tag{5}$$

where $(n_B)_i$ and $(n_F)_i$ are the bearing and frequency measurement errors. The equations (4) and (5) can be written as a single equation in vector form

$$\boldsymbol{\gamma}^m = \boldsymbol{\gamma}(\mathbf{a}_B) + \mathbf{n}_B \tag{6}$$

and

$$\boldsymbol{\nu}^m = \boldsymbol{\nu}(\mathbf{a}_F) + \mathbf{n}_F. \tag{7}$$

The measurement errors $\mathbf{n}_B$ and $\mathbf{n}_F$ are multivariate random M_B-dimensional and M_F-dimensional vectors with covariance matrices

$$\mathbf{N}_B = E[(\mathbf{n}_B - E[\mathbf{n}_B])(\mathbf{n}_B - E[\mathbf{n}_B])^T] \tag{8}$$

and

$$\mathbf{N}_F = E[(\mathbf{n}_F - E[\mathbf{n}_F])(\mathbf{n}_F - E[\mathbf{n}_F])^T] \tag{9}$$

respectively, where $E[\ ]$ denotes the expected value.

Combining the bearing and frequency measurements (6) and (7) to form a single set of $M_c = M_B + M_F$ measurements, we obtain the measurement equation of CM:

$$\boldsymbol{\mu}^m = \boldsymbol{\mu}(\mathbf{a}_c) + \mathbf{n}_c \tag{10}$$

where

$$\boldsymbol{\mu}^m = \begin{pmatrix}\boldsymbol{\gamma}^m\\ \boldsymbol{\nu}^m\end{pmatrix}; \qquad \boldsymbol{\mu}(\mathbf{a}_c) = \begin{pmatrix}\boldsymbol{\gamma}(\mathbf{a}_B)\\ \boldsymbol{\nu}(\mathbf{a}_F)\end{pmatrix}; \qquad \mathbf{n}_c = \begin{pmatrix}\mathbf{n}_B\\ \mathbf{n}_F\end{pmatrix}. \tag{11}$$

Obviously $\mathbf{a}_c = \mathbf{a}_F$. Since the bearing and frequency measurements are independent of each other the

$M_c \times M_c$ covariance matrix $\mathbf{N}_c$ of $\mathbf{n}_c$ is a matrix of the block-diagonal form

$$\mathbf{N}_C = \begin{pmatrix} \mathbf{N}_B & \mathbf{0} \\ \mathbf{0} & \mathbf{N}_F \end{pmatrix}. \tag{12}$$

Some of the following relations are formally identical for BM, FM, and CM, and there is no need for distinguishing them explicitly. For notational convenience the subscripts B, F, and C are omitted in these cases. Thus, $\mathbf{n}$ for instance may denote $\mathbf{n}_B$, $\mathbf{n}_F$, or $\mathbf{n}_C$, the actual meaning being clear from the context. The same is true for the parameter vector $\mathbf{a}$, the covariance $\mathbf{N}$, etc. In this notation, the measurement equations (6), (7), and (11) for instance condense into the single equation

$$\psi^m = \psi(\mathbf{a}) + \mathbf{n} \tag{13}$$

where

$$\psi(\mathbf{a}) = \begin{cases} \gamma(\mathbf{a}_B) & \text{for BM} \\ \nu(\mathbf{a}_F) & \text{for FM} \\ \mu(\mathbf{a}_c) & \text{for CM} \end{cases}. \tag{14}$$

For explicit parameter estimation the distribution of the measurement error $\mathbf{n}$ must be known. In principle, measurements are subject to both random and systematic errors. In what follows, it is assumed that no systematic error is present, and that the errors in the bearing and frequency measurements can be adequately described by zero mean normal probability distributions. In addition, it is assumed that the measurements are independent of each other and that the variances are independent of the measurement points, i.e., $(N_B)_{ii} \boxminus \sigma_B^2$, and $(N_F)_{ii} \equiv \sigma_F^2$. The latter are reasonable assumptions if the sampling frequency is not too high and if the measurement points are much closer to each other than to the emitter. Accordingly the conditional density of ψ^m given $\mathbf{a}$ is the multivariate normal density

$$p(\psi^m \mid \mathbf{a}) = \frac{1}{(2\pi)^{M/2}\sqrt{\det \mathbf{N}}} \times \exp\left(-\frac{1}{2}\sum_{i=1}^{M} \frac{[\psi_i^m - \psi_i(\mathbf{a})]^2}{N_{ii}}\right) \tag{15}$$

where $\det \mathbf{N}$ denotes the determinant of $\mathbf{N}$.

III. CRAMER–RAO ANALYSIS

In judging an estimation problem, it is important to know the maximum estimation accuracy that can be attained with the measurements. As is well known, the CR bounds provide powerful lower bounds on the estimation accuracy (see e.g., [12]). Further, since they are lower bounds for any estimator, their parameter dependences reveal characteristic features of the estimation problem.

In its multidimensional form the CR inequality states: Let $\mathbf{a}$ be an unknown parameter vector of dimension n and let $\hat{\mathbf{a}}(\psi^m)$ denote some unbiased estimate of $\mathbf{a}$ based on the measurements ψ^m. If $\mathbf{C}$ denotes the covariance matrix of the estimation error

$$\widehat{\Delta \mathbf{a}} = \hat{\mathbf{a}}(\psi^m) - \mathbf{a} \tag{16}$$

then

$$\mathbf{C} \geq \mathbf{J}^{-1} \tag{17}$$

where

$$J_{kl} = -E\left[\frac{\partial^2 \ln p(\psi^m \mid \mathbf{a})}{\partial a_k \, \partial a_l}\right], \qquad 1 \leq k,l \leq n \tag{18}$$

are the elements of the matrix $\mathbf{J}$. $\mathbf{J}$ is known as the Fisher information matrix, and its inverse (the right-hand side of (17)) is the CR bound. The matrix inequality (17) between the two symmetric matrices $\mathbf{C}$ and $\mathbf{J}^{-1}$ denotes that $\mathbf{C} - \mathbf{J}^{-1}$ is nonnegative definite.

Geometrically, the covariance matrix $\mathbf{C}$ can be visualized in the space of the estimation error by the concentration ellipsoid

$$\widehat{\Delta \mathbf{a}}^T \mathbf{C}^{-1} \widehat{\Delta \mathbf{a}} = \kappa \tag{19}$$

where κ is a constant that determines the size of the n-dimensional region enclosed by the surface. In these terms an equivalent formulation of the CR inequality reads: For any unbiased estimate of $\mathbf{a}$ the concentration ellipsoid (19) lies outside or on the bound ellipsoid defined by

$$\widehat{\Delta \mathbf{a}}^T \mathbf{J} \widehat{\Delta \mathbf{a}} = \kappa. \tag{20}$$

We concentrate on this version of the CR inequality in this study since for an intuitive understanding of the location methods it is more enlightening than the formal relation (17).

The size and orientation of the ellipsoid (20) can be best described in terms of the eigenvalues and eigenvectors of the symmetric $n \times n$ matrix $\mathbf{J}$. To this end the eigenvalue problem

$$\mathbf{J}\xi_i = \lambda_i \xi_i, \qquad i = 1,\ldots,n \tag{21}$$

has to be solved, where $\lambda_1,\ldots,\lambda_n$ are the eigenvalues of $\mathbf{J}$ and $\xi_1,\ldots,\xi_n$ the corresponding eigenvectors. The mutually orthogonal eigenvectors coincide with the principal axes of the bound ellipsoid and form an orthogonal matrix $\mathbf{A} = (\xi_1,\ldots,\xi_n)$ that diagonalizes $\mathbf{J}$

$$\mathbf{A}^T \mathbf{J} \mathbf{A} = \begin{pmatrix} \lambda_1 & & 0 \\ & \ddots & \\ 0 & & \lambda_n \end{pmatrix}. \tag{22}$$

Thus, rotating the coordinate axes by means of the transformation $\mathbf{A}^T$ in the new variables defined by

$$\zeta = \mathbf{A}^T \widehat{\Delta \mathbf{a}} \tag{23}$$

the ellipsoid (20) takes the form

$$\widehat{\Delta \mathbf{a}}^T \mathbf{J} \widehat{\Delta \mathbf{a}} = \sum_{i=1}^{n} \lambda_i \zeta_i^2 = \kappa. \tag{24}$$

This is in the coordinates ζ_i the equation of an ellipsoid in its standard form with semiaxes of length $\sqrt{\kappa/\lambda_i}$. If some $\lambda_i = 0$, then the value of the corresponding coordinate ζ_i can be chosen arbitrarily, i.e., (24) describes a degenerate ellipsoid extending to infinity in this coordinate direction.

The Fisher information matrix exhibits the information contents of the estimation problem. Thus, physically $\lambda_i = 0$ means that there is no information at all about the corresponding coordinate ζ_i, i.e., ζ_i is unobservable.

For the location problem considered in this study the Fisher information matrix is obtained from the conditional density (15). Taking the logarithm and differentiating (18) yields

$$J_{kl} = \sum_{i=1}^{M} \frac{1}{N_{ii}} \frac{\partial \psi_i}{\partial a_k} \frac{\partial \psi_i}{\partial a_l} \tag{25}$$

or in matrix form

$$\mathbf{J} = \sum_{i=1}^{M} \frac{1}{N_{ii}} \nabla_{\mathbf{a}} \psi_i (\nabla_{\mathbf{a}} \psi_i)^T \tag{26}$$

where $\nabla_{\mathbf{a}}$ denotes the gradient with respect to $\mathbf{a}$. Specifically,

$$\begin{aligned} \nabla_{\mathbf{a}_B} \gamma_i &= \left(\frac{\partial \gamma_i}{\partial x_e}, \frac{\partial \gamma_i}{\partial y_e} \right)^T \\ &= \frac{1}{|\mathbf{r}_e - \mathbf{r}_i|^2} \begin{pmatrix} y_i - y_e \\ x_e - x_i \end{pmatrix} \end{aligned} \tag{27}$$

$$\begin{aligned} \nabla_{\mathbf{a}_F} \nu_i &= \left(\frac{\partial \nu_i}{\partial \nu_0}, \frac{\partial \nu_i}{\partial x_e}, \frac{\partial \nu_i}{\partial y_e} \right)^T \\ &= \begin{pmatrix} 1 + \dfrac{1}{c|\mathbf{r}_e - \mathbf{r}_i|} [\dot{x}_i (x_e - x_i) + \dot{y}_i (y_e - y_i)] \\ \dfrac{\nu_0}{c} \dfrac{y_e - y_i}{|\mathbf{r}_e - \mathbf{r}_i|^3} [\dot{x}_i (y_e - y_i) - \dot{y}_i (x_e - x_i)] \\ \dfrac{\nu_0}{c} \dfrac{x_e - x_i}{|\mathbf{r}_e - \mathbf{r}_i|^3} [\dot{y}_i (x_e - x_i) - \dot{x}_i (y_e - y_i)] \end{pmatrix} \end{aligned} \tag{28}$$

and according to the particular arranging of the bearing and frequency measurements in (11)

$$\nabla_{\mathbf{a}_c} \mu_i = \begin{cases} \begin{pmatrix} 0 \\ \nabla_{\mathbf{a}_B} \gamma_i \end{pmatrix} & \text{for } 1 \le i \le M_B \\ \nabla_{\mathbf{a}_F} \nu_i & \text{for } i > M_B \end{cases}. \tag{29}$$

Consequently, in BM the estimation error bound (20) is an ellipse in position space, whereas in FM and CM the bound is an ellipsoid in the three-dimensional space of position and frequency coordinates. Naturally,

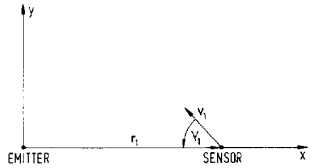

Fig. 2. Initial sensor-emitter geometry.

in a location system the position estimates are of main importance. Therefore, in FM and CM the location error irrespective of the frequency estimation is of major interest here. Obviously, a bound on this error is provided by the position space submatrix of $\mathbf{J}^{-1}$ (cf. (17)). The corresponding bound ellipse is given by

$$(\mathbf{P}\widehat{\Delta \mathbf{a}})^T (\mathbf{P}\mathbf{J}^{-1}\mathbf{P}^T)^{-1} \mathbf{P}\widehat{\Delta \mathbf{a}} = \kappa \tag{30}$$

where $\mathbf{P}$ denotes the projection operator

$$\mathbf{P} = \begin{pmatrix} 0 & 1 & 0 \\ 0 & 0 & 1 \end{pmatrix} \tag{31}$$

which projects the three-dimensional frequency-position space with coordinates (ν, x, y) onto the two-dimensional subspace of position coordinates (x, y). Geometrically, the ellipse defined by (30) is the projection of the ellipsoid (20) onto the two-dimensional position space.

In principle, the maximum location accuracy of BM, FM, and CM can now be assessed in this way for an arbitrary number of measurements taken along arbitrarily chosen sensor trajectories. Though useful in evaluating definite sensor-emitter scenarios, the multimeasurement case, however, does not provide a deeper insight into the location methods because of its vast number of parameters. The number of parameters drastically reduces if only one single measurement is considered. Since the position estimate is derived from measurements taken successively along the sensor trajectory an investigation of the single measurement influence provides an insight into the mechanism of the estimation process and into sensor trajectory shapes which are favorable for position location as well.

The single measurement case is studied in the next subsections. Without loss of generality the calculations can be performed in a system of coordinates with the origin at the emitter and the x-axis aligned with the initial LOS (Fig. 2).

A. One Single Bearing Measurement

From (26) the Fisher information matrix of a single bearing measurement is given by

$$\mathbf{J} = \frac{1}{\sigma_B^2} \nabla_{\mathbf{a}_B} \gamma (\nabla_{\mathbf{a}_B} \gamma)^T \tag{32}$$

where in the formula the measurement index has been omitted for convenience. In the coordinate system

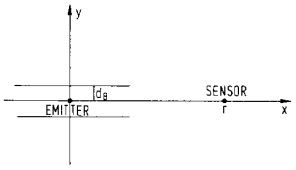

Fig. 3. Degenerate bound ellipse (20) in single bearing measurement case.

defined by Fig. 2, (27) simplifies to

$$\nabla_{\mathbf{a}_B}\gamma = \frac{1}{r}\begin{pmatrix} 0 \\ -1 \end{pmatrix}. \tag{33}$$

Accordingly, the matrix (32) takes the simple form

$$\mathbf{J} = \frac{1}{\sigma_B^2 r^2}\begin{pmatrix} 0 & 0 \\ 0 & 1 \end{pmatrix}. \tag{34}$$

By inspection, the eigenvectors and eigenvalues are

$$\xi_1 = \begin{pmatrix} 1 \\ 0 \end{pmatrix}; \qquad \xi_2 = \begin{pmatrix} 0 \\ 1 \end{pmatrix} \tag{35}$$

and

$$\lambda_1 = 0; \qquad \lambda_2 = \frac{1}{\sigma_B^2 r^2} \tag{36}$$

respectively. Therefore, from the above discussion the estimation error bound (20) is a degenerate ellipse with semimajor axis of infinite length in the direction of ξ_1 (LOS) and semiminor axis of length

$$d_B = \sigma_B r\sqrt{\kappa} \tag{37}$$

perpendicular to LOS. Thus, graphically each bearing measurement is associated with a strip of infinite length in the direction of LOS and of width $2d_B$ perpendicular to it (Fig. 3). In this picture the estimation error ellipse of the multimeasurement case can be interpreted as the result of the intersection of the individual strips. Thereby an intuitive understanding of BM has been gained.

B. Frequency Measurements

1) *One Single Frequency Measurement*: The Fisher information matrix of the single frequency measurement case is given by

$$\mathbf{J} = \frac{1}{\sigma_F^2}\nabla_{\mathbf{a}_F}\nu(\nabla_{\mathbf{a}_F}\nu)^T. \tag{38}$$

In the coordinate system under consideration (Fig. 2) the gradient (28) now takes the form

$$\nabla_{\mathbf{a}_F}\nu = \begin{pmatrix} 1 + \frac{v}{c}\cos\gamma \\ \frac{\nu_0 v}{cr}\sin\gamma \end{pmatrix}. \tag{39}$$

Hence

$$\mathbf{J} = \frac{\nu_0^2}{\sigma_F^2}\Gamma \tag{40}$$

where

$$\Gamma = \begin{pmatrix} u^2 & 0 & uw \\ 0 & 0 & 0 \\ uw & 0 & w^2 \end{pmatrix} \tag{41}$$

and

$$u = \frac{1}{\nu_0}\left(1 + \frac{v}{c}\cos\gamma\right); \qquad w = \frac{v}{cr}\sin\gamma. \tag{42}$$

From the characteristic equation of Γ we obtain the 3 eigenvalues

$$\begin{aligned} \lambda_1 &= u^2 + w^2 \\ \lambda_{2,3} &= 0. \end{aligned} \tag{43}$$

Substituting them into the eigenvector equation, the corresponding eigenvectors result:

$$\begin{aligned} \xi_1 &= \frac{1}{\sqrt{u^2+w^2}}\begin{pmatrix} u \\ 0 \\ w \end{pmatrix}; \\ \xi_2 &= \begin{pmatrix} 0 \\ 1 \\ 0 \end{pmatrix}; \\ \xi_3 &= \frac{1}{\sqrt{u^2+w^2}}\begin{pmatrix} -w \\ 0 \\ u \end{pmatrix}. \end{aligned} \tag{44}$$

These define the orthogonal matrix $\mathbf{A} = (\xi_1, \xi_2, \xi_3)$ that diagonalizes $\mathbf{J}$:

$$\mathbf{A}^T\mathbf{J}\mathbf{A} = \frac{\nu_0^2}{\sigma_F^2}\begin{pmatrix} u^2+w^2 & 0 & 0 \\ 0 & 0 & 0 \\ 0 & 0 & 0 \end{pmatrix}. \tag{45}$$

Thus, in the single frequency measurement case the estimation error bound (20) describes a degenerate ellipsoid with semiaxes of infinite length in the direction of ξ_2 (LOS) and ξ_3 and of length

$$d_1 = \frac{\sigma_F\sqrt{\kappa}}{\nu_0\sqrt{u^2+w^2}} \tag{46}$$

in the direction of ξ_1. The bound can be illustrated in the frequency-position space as an infinitely extending disk of width $2d_1$ rotated by an angle ϑ about the LOS (Fig. 4).

From Fig. 4

$$\begin{aligned} \cos\vartheta &= \xi_1 \cdot \mathbf{e}_y \\ &= \frac{w}{\sqrt{u^2+w^2}} \end{aligned} \tag{47}$$

where $\mathbf{e}_y$ is the unit vector in the direction of the y-axis. Since u does not vanish ($v/c < 1$), the rotation angle ϑ always is different from zero. Thus, apart from $\gamma = 0$ and $\gamma = \pi$ where $\vartheta = \pi/2$, there is always

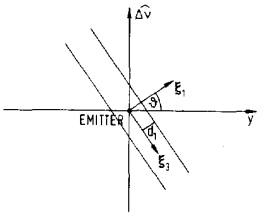

Fig. 4. Degenerate bound ellipsoid (20) in single frequency measurement case.

a correlation between the position and frequency estimation errors.

It is now shown, how the disk in the frequency-position space affects the location accuracy independent of frequency estimation. A bound on that accuracy is given by (30). In the single frequency measurement case, however, (30) cannot be directly evaluated, since the inverse of (40) does not exist. But this problem can be overcome, if the singular J is considered as the limiting case of a regular matrix. One possible choice for a regular matrix with the wanted limiting property for instance is

$$\mathbf{J}(\epsilon) = \frac{\nu_0^2}{\sigma_F^2}\mathbf{\Gamma}(\epsilon) \tag{48}$$

where

$$\mathbf{\Gamma}(\epsilon) = \begin{pmatrix} u^2 & 0 & uw \\ 0 & \epsilon & 0 \\ uw & 0 & w^2+\epsilon \end{pmatrix} \tag{49}$$

for $\lim_{\epsilon\to 0}\mathbf{J}(\epsilon) = \mathbf{J}$ and $\det\mathbf{\Gamma}(\epsilon) = u^2\epsilon^2 \neq 0$. Now,

$$\mathbf{J}^{-1}(\epsilon) = \frac{\sigma_F^2}{\nu_0^2}\frac{\mathrm{adj}\mathbf{\Gamma}(\epsilon)}{\det\mathbf{\Gamma}(\epsilon)} \tag{50}$$

where $\mathrm{adj}\mathbf{\Gamma}(\epsilon)$ denotes the adjoint of $\mathbf{\Gamma}(\epsilon)$. For the evaluation of (30) the inverse of the position space submatrix of $\mathbf{J}^{-1}$ is needed. Substituting

$$\mathbf{P}\,\mathrm{adj}\mathbf{\Gamma}(\epsilon)\mathbf{P}^T = \begin{pmatrix} u^2\epsilon & 0 \\ 0 & u^2\epsilon \end{pmatrix} \tag{51}$$

into (50) and inverting we finally obtain

$$(\mathbf{P}\mathbf{J}^{-1}(\epsilon)\mathbf{P}^T)^{-1} = \frac{\nu_0^2}{\sigma_F^2}\begin{pmatrix} \epsilon & 0 \\ 0 & \epsilon \end{pmatrix}. \tag{52}$$

Since both eigenvalues of the matrix (52) tend to zero, the location bound in the single frequency measurement case is the whole position space. This is in agreement with the geometrical interpretation of (30) as the projection of the ellipsoid (20) (here the disk) onto the position space.

2) *Two Frequency Measurements*: As opposed to the single bearing measurement case, a single frequency measurement does not provide any distinct bound in the position space. Two frequency measurements, however, intuitively lead to an intersection of the two disks associated with the

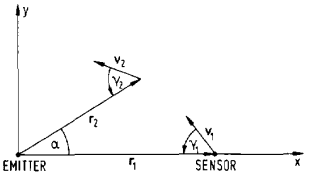

Fig. 5. Sensor-emitter geometry for 2 arbitrary points on sensor trajectory and arbitrary sensor velocities.

single measurements. Since the projection of the intersecting region onto the position space is a strip of infinite length, this gives the idea that two frequency measurements presumably will provide a bound in position space comparable to that of a single bearing measurement.

From (26) the Fisher information matrix for two frequency measurements is

$$\mathbf{J} = \frac{1}{\sigma_F^2}\sum_{i=1}^{2}\nabla_{\mathbf{a}_F}\nu_i(\nabla_{\mathbf{a}_F}\nu_i)^T. \tag{53}$$

In the coordinate system of Fig. 2 the gradient of ν_1 is given by (39) and the gradient of ν_2 by

$$\nabla_{\mathbf{a}_F}\nu_2 = \begin{pmatrix} 1+\dfrac{v_2}{c}\cos\gamma_2 \\ -\nu_0\dfrac{v_2}{cr_2}\sin\gamma_2\sin\alpha \\ \nu_0\dfrac{v_2}{cr_2}\sin\gamma_2\cos\alpha \end{pmatrix} \tag{54}$$

(Fig. 5). Hence

$$\mathbf{J} = \frac{\nu_0^2}{\sigma_F^2}\cdot\mathbf{\Gamma} \tag{55}$$

where

$$\mathbf{\Gamma} = \begin{pmatrix} u_1^2+u_2^2 & -u_2w_2\sin\alpha & u_1w_1+u_2w_2\cos\alpha \\ -u_2w_2\sin\alpha & w_2^2\sin^2\alpha & -w_2^2\sin\alpha\cos\alpha \\ u_1w_1+u_2w_2\cos\alpha & -w_2^2\sin\alpha\cos\alpha & w_1^2+w_2^2\cos^2\alpha \end{pmatrix} \tag{56}$$

and

$$\begin{aligned} u_i &= \frac{1}{\nu_0}\left(1+\frac{v_i}{c}\cos\gamma_i\right), \qquad i=1,2 \\ w_i &= \frac{v_i}{cr_i}\sin\gamma_i, \qquad i=1,2. \end{aligned} \tag{57}$$

Following the lines of the preceding sections the matrix (55) can be diagonalized by solving the eigenvalue problem. Some straightforward calculation leads to the 3 eigenvalues of $\mathbf{\Gamma}$

$$\begin{aligned} \lambda_1 &= 0 \\ \lambda_2 &= p+\sqrt{p^2-q} \\ \lambda_3 &= p-\sqrt{p^2-q} \end{aligned} \tag{58}$$

where

$$p = \tfrac{1}{2}(u_1^2 + u_2^2 + w_1^2 + w_2^2)$$

$$q = u_1^2 w_2^2 + u_2^2 w_1^2 + w_1^2 w_2^2 \sin^2\alpha - 2u_1 u_2 w_1 w_2 \cos\alpha. \tag{59}$$

The corresponding eigenvectors are

$$\xi_1 = \frac{1}{\sqrt{q}} \begin{pmatrix} -w_1 w_2 \sin\alpha \\ u_1 w_2 \cos\alpha - u_2 w_1 \\ u_1 w_2 \sin\alpha \end{pmatrix} \tag{60}$$

$$\xi_i = \frac{\xi_i'}{|\xi_i'|}, \qquad i = 2,3$$

where

$$\xi_i' = \begin{pmatrix} (u_1 w_1 + u_2 w_2 \cos\alpha)\lambda_i - u_1 w_1 w_2^2 \sin^2\alpha \\ u_1 \sin\alpha (u_1 w_2^2 \cos\alpha - u_2 w_1 w_2) - \lambda_i w_2^2 \sin\alpha \cos\alpha \\ (w_1^2 + w_2^2 \cos^2\alpha)\lambda_i + u_1^2 w_2^2 \sin^2\alpha - q \end{pmatrix}. \tag{61}$$

By means of a similarity transformation with the orthogonal matrix $\mathbf{A} = (\xi_1, \xi_2, \xi_3)$ we obtain

$$\mathbf{A}^T \mathbf{J} \mathbf{A} = \frac{\nu_0^2}{\sigma_F^2} \begin{pmatrix} 0 & 0 & 0 \\ 0 & p + \sqrt{p^2 - q} & 0 \\ 0 & 0 & p - \sqrt{p^2 - q} \end{pmatrix}. \tag{62}$$

Thus, in the case of two frequency measurements, (20) describes a degenerate ellipsoid with semiaxes of infinite length in the direction of ξ_1 and of length

$$d_2 = \frac{\sigma_F \sqrt{\kappa}}{\nu_0 \sqrt{p + \sqrt{p^2 - q}}}$$

$$d_3 = \frac{\sigma_F \sqrt{\kappa}}{\nu_0 \sqrt{p - \sqrt{p^2 - q}}} \tag{63}$$

in the direction of ξ_2 and ξ_3, respectively.

From (62) we immediately conclude that $\mathbf{J}$ is singular. Therefore, for an evaluation of the location accuracy bound (30) we proceed in a way analogous to the single frequency measurement case. Instead of (55) we now consider the matrix

$$\mathbf{J}(\epsilon) = \frac{\nu_0^2}{\sigma_F^2} \boldsymbol{\Gamma}(\epsilon) \tag{64}$$

where

$$\boldsymbol{\Gamma}(\epsilon) = \begin{pmatrix} u_1^2 + u_2^2 & -u_2 w_2 \sin\alpha & u_1 w_1 + u_2 w_2 \cos\alpha \\ -u_2 w_2 \sin\alpha & \epsilon + w_2^2 \sin^2\alpha & -w_2^2 \sin\alpha \cos\alpha \\ u_1 w_1 + u_2 w_2 \cos\alpha & -w_2^2 \sin\alpha \cos\alpha & \epsilon + w_1^2 + w_2^2 \cos^2\alpha \end{pmatrix}. \tag{65}$$

Since

$$\det \boldsymbol{\Gamma}(\epsilon) = \epsilon[(u_1 w_2 \cos\alpha - u_2 w_1)^2 + u_1^2 w_2^2 \sin^2\alpha + \epsilon(u_1^2 + u_2^2)] \tag{66}$$

is different from zero, (64) obviously is a regular matrix with the wanted limiting property $\lim_{\epsilon \to 0} \mathbf{J}(\epsilon) = \mathbf{J}$. Now, the position space submatrix $\mathbf{P}\mathbf{J}^{-1}(\epsilon)\mathbf{P}^T$ can be calculated. Taking its inverse we finally obtain after some straightforward calculation

$$(\mathbf{P}\mathbf{J}^{-1}(\epsilon)\mathbf{P}^T)^{-1} = \frac{\nu_0^2}{\sigma_F^2 (u_1^2 + u_2^2)} \begin{pmatrix} \epsilon(u_1^2 + u_2^2) + u_1^2 w_2^2 \sin^2\alpha & -(u_1 w_2 \cos\alpha - u_2 w_1) u_1 w_2 \sin\alpha \\ -(u_1 w_2 \cos\alpha - u_2 w_1) u_1 w_2 \sin\alpha & \epsilon(u_1^2 + u_2^2) + (u_1 w_2 \cos\alpha - u_2 w_1)^2 \end{pmatrix}. \tag{67}$$

This approaches in the limit $\epsilon \to 0$ a matrix with eigenvalues

$$s_1 = 0$$

$$s_2 = \frac{\nu_0^2}{\sigma_F^2 (u_1^2 + u_2^2)} [u_1^2 w_2^2 \sin^2\alpha + (u_1 w_2 \cos\alpha - u_2 w_1)^2] \tag{68}$$

and corresponding eigenvectors

$$\eta_1 = \frac{1}{\sqrt{u_1^2 w_2^2 \sin^2\alpha + (u_1 w_2 \cos\alpha - u_2 w_1)^2}} \times \begin{pmatrix} u_1 w_2 \cos\alpha - u_2 w_1 \\ u_1 w_2 \sin\alpha \end{pmatrix}$$

$$\eta_2 = \frac{1}{\sqrt{u_1^2 w_2^2 \sin^2\alpha + (u_1 w_2 \cos\alpha - u_2 w_1)^2}} \times \begin{pmatrix} -u_1 w_2 \sin\alpha \\ u_1 w_2 \cos\alpha - u_2 w_1 \end{pmatrix}. \tag{69}$$

Thus, as expected, the bound on the location accuracy associated with two frequency measurements is a degenerate ellipse with semimajor axis of infinite length in the direction of η_1 and semiminor axis of length

$$d_F = \sqrt{\frac{\kappa}{s_2}} \tag{70}$$

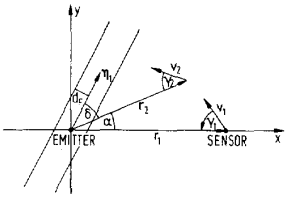

Fig. 6. Lower bound on location error in the case of 2 frequency measurements.

in the direction of η_2. It can be illustrated as a strip of width $2d_F$ and of infinite length in the direction of η_1. Geometrically, this is the projection of the degenerate ellipsoid in the frequency-position space onto the position space (compare e.g., the components of ξ_1 with those of η_1).

Note that the strip is rotated by an angle δ with respect to the LOS at the last measurement point (Fig. 6). This is a characteristic feature of FM and is qualitatively different from BM where the strips are aligned with LOS. As can be seen from the cross product $\mathbf{r}_2 \times \eta_1$ the rotation is counterclockwise as long as $0 \le \alpha, \gamma_1, \gamma_2 \le \pi$. From Fig. 6 we conclude that

$$\cos\delta = \frac{\mathbf{r}_2}{r_2} \cdot \eta_1 = \frac{u_1 w_2 - u_2 w_1 \cos\alpha}{\sqrt{u_1^2 w_2^2 \sin^2\alpha + (u_1 w_2 \cos\alpha - u_2 w_1)^2}}. \quad (71)$$

Substituting (57) into (71) we immediately see that δ is a function of the geometric parameters (α, r_1, r_2) and of the dynamical parameters $(v_1, v_2, \gamma_1, \gamma_2)$ as well. Let $(\alpha, r_1, r_2, v_1, v_2, \gamma_1)$ be a given set of parameters and let $0 \le \alpha \le \pi$, then it can be shown that for $0 \le \gamma_2 \le \pi$ the angle δ first is a monotonically decreasing function of γ_2, attains its minimum at $\gamma_{\min} = \cos^{-1}(-v_2/c)$, and is monotonically increasing up to the initial value $\delta(\gamma_2 = 0)$ again. Thus, the maximum value of rotation is

$$\delta_{\max} = \pi - \alpha. \quad (72)$$

Since $\gamma_{\min} \approx \pi/2$ $(v_2/c \approx 0)$ the minimum value approximately is

$$\delta_{\min} \approx \cos^{-1}\left[\frac{1 - g\cos\alpha}{\sqrt{1 - 2g\cos\alpha + g^2}}\right] \quad (73)$$

where

$$g = \frac{v_1 r_2 \sin\gamma_1}{v_2 r_1 \left(1 + \frac{v_1}{c}\cos\gamma_1\right)}. \quad (74)$$

Consequently the orientation of the strip can be controlled over a wide range of angles by a sensor maneuver (γ_2). Especially, if $\alpha < \pi/2$ and $1 - g\cos\alpha > 0$ (as is usually the case for an approaching sensor) there always will be a maneuver γ_2 so that the strip associated with two frequency measurements is perpendicular to the LOS at the last measurement point. The angle in this case can be determined from $u_1 w_2 = u_2 w_1 \cos\alpha$ (cf., (71)).

The width of the strip is given by $2d_F$ (70). According to (68) it is just like δ, a function of the geometric and dynamic parameters and can also be controlled over a wide range by appropriate sensor maneuvers. The parametric dependences, however, now are more involved than for the rotation angle δ.

C. Combined Set of Bearing and Frequency Measurements

As has been shown the strips resulting from two frequency measurements are rotated with respect to the LOS at the last measurement point. As a consequence the directions of the principal axes of the bound ellipses (30) for BM and FM do not coincide. From this we expect a significant enhancement of location accuracy by simultaneous processing of bearing and frequency measurements.

In the following the gain of CM in relation to BM and FM is investigated. To this end we consider the location estimation error bounds (30) resulting from a given set of bearing and frequency measurements. According to (30) these are obtained from the 2×2 matrices $\mathbf{J}_B$, $(\mathbf{P}\mathbf{J}_F^{-1}\mathbf{P}^T)^{-1}$, and $(\mathbf{P}\mathbf{J}_C^{-1}\mathbf{P}^T)^{-1}$, respectively.

Now, let the bound ellipses for BM and FM be the two ellipses E_B and E_F of Fig. 7. They are rotated with respect to each other by an angle φ. Obviously the corresponding bound ellipse E_C of CM can be written in terms of the ellipses E_B and E_F. From (26) and (29) we conclude that

$$(\mathbf{P}\mathbf{J}_c^{-1}\mathbf{P}^T)^{-1} = \mathbf{J}_B + (\mathbf{P}\mathbf{J}_F^{-1}\mathbf{P}^T)^{-1}. \quad (75)$$

According to Fig. 7 and (24) in the coordinate system in which $\mathbf{J}_B$ is diagonal the matrices $\mathbf{J}_B$ and $(\mathbf{P}\mathbf{J}_F^{-1}\mathbf{P}^T)^{-1}$ take the form

$$\mathbf{J}_B = \begin{pmatrix} \frac{\kappa}{e_B^2} & 0 \\ 0 & \frac{\kappa}{f_B^2} \end{pmatrix} \quad (76)$$

and

$$(\mathbf{P}\mathbf{J}_F^{-1}\mathbf{P}^T)^{-1} = \mathbf{D}(-\varphi) \begin{pmatrix} \frac{\kappa}{e_F^2} & 0 \\ 0 & \frac{\kappa}{f_F^2} \end{pmatrix} \mathbf{D}(\varphi) \quad (77)$$

where

$$\mathbf{D}(\varphi) = \begin{pmatrix} \cos\varphi & \sin\varphi \\ -\sin\varphi & \cos\varphi \end{pmatrix}. \quad (78)$$

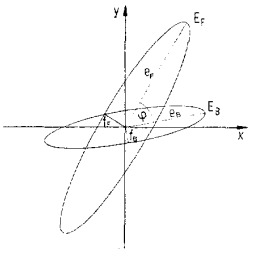

Fig. 7. Rotated location estimation error bounds of BM and FM.

Adding (76) and (77) we obtain

$$(\mathbf{P}\mathbf{J}_C^{-1}\mathbf{P}^T)^{-1} = \kappa \begin{pmatrix} \frac{1}{e_B^2} + \frac{\cos^2\varphi}{e_F^2} + \frac{\sin^2\varphi}{f_F^2} & \left(\frac{1}{e_F^2} - \frac{1}{f_F^2}\right)\sin\varphi\cos\varphi \\ \left(\frac{1}{e_F^2} - \frac{1}{f_F^2}\right)\sin\varphi\cos\varphi & \frac{1}{f_B^2} + \frac{\sin^2\varphi}{e_F^2} + \frac{\cos^2\varphi}{f_F^2} \end{pmatrix}. \tag{79}$$

When inserted into (30) this provides the bound ellipse E_C, its size and orientation being determined by the eigenvalues λ_1, λ_2 and the eigenvectors ξ_1, ξ_2 of the matrix (79). Since the semiaxes of the ellipse E_C are of length $e_c = \sqrt{\kappa/\lambda_1}$ and $f_c = \sqrt{\kappa/\lambda_2}$, the area A_C of E_C equals

$$A_C = \frac{\pi\kappa}{\sqrt{\lambda_1\lambda_2}} = \frac{\pi\kappa}{\sqrt{\det[(\mathbf{P}\mathbf{J}_C^{-1}\mathbf{P}^T)^{-1}]}} = \frac{\pi e_B f_B e_F f_F}{\sqrt{(e_B^2+e_F^2)(f_B^2+f_F^2)+(e_B^2-f_B^2)(e_F^2-f_F^2)\sin^2\varphi}}. \tag{80}$$

Now, the ratio A_B/A_C of the area of the ellipses E_B and E_C is a measure for the location gain by CM in relation to BM. We obtain

$$G = \frac{A_B}{A_C} = \frac{\sqrt{(e_B^2+e_F^2)(f_B^2+f_F^2)+(e_B^2-f_B^2)(e_F^2-f_F^2)\sin^2\varphi}}{e_F f_F}. \tag{81}$$

The gain G is made up of two components: first the gain resulting from the rotation φ

$$G_\varphi = \frac{A_C(\varphi=0)}{A_C(\varphi)} = \sqrt{1+\frac{(e_B^2-f_B^2)(e_F^2-f_F^2)}{(e_B^2+e_F^2)(f_B^2+f_F^2)}\sin^2\varphi} \tag{82}$$

and second the statistical gain resulting from the combination of two unrotated ellipses based on independent measurements

$$G_{ST} = \frac{A_B}{A_C(\varphi=0)} = \frac{\sqrt{(e_B^2+e_F^2)(f_B^2+f_F^2)}}{e_F f_F}. \tag{83}$$

Obviously

$$G = G_\varphi \cdot G_{ST}. \tag{84}$$

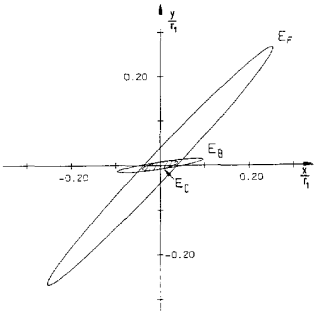

Fig. 8. Location error bounds (30) for BM, FM, and CM; $\nu_0 = 3$ GHz, $r_1 = 10$ km, $v = 300$ m/s, $\gamma_1 = 50°$, $1/\Delta t = 10$ Hz, $\sigma_B = 5°$, $\sigma_F = 100$ Hz, 100 measurement points.

For a demonstration of the attainable location accuracies let us consider a stationary radar operating at a frequency $\nu_0 = 3$ GHz and a sensor moving inertially with velocity $v = 300$ m/s. The initial aspect angle and the initial radar sensor distance are assumed to be $\gamma_1 = 50°$ and $r_1 = 10$ km, respectively. Over a distance of 3 km bearing and frequency measurements are taken at a constant sampling rate $1/\Delta t = 10$ Hz. The errors are assumed to be normally distributed with zero mean and standard deviation $\sigma_B = 5°$ and $\sigma_F = 100$ Hz, respectively. In Fig. 8 the resulting error bounds for BM, FM, and CM are depicted ($\kappa = 1$). As can be seen, the location accuracy bound for CM is considerably smaller than for BM and FM. For the gains we obtain: $G = 2.44$, $G_\varphi = 2.26$, $G_{ST} = 1.08$. This indicates that the main contribution to the gain in location accuracy is due to the rotation of E_F with respect to E_B ($\varphi = 38.4°$).

IV. SIMULATION RESULTS

The results so far specify properties of the location methods from an analysis of the CR lower bounds. Now, the question arises whether and to what extent these properties show up again in specific estimation procedures, even if the assumption of an unbiased estimate is not always exactly fulfilled. This has been investigated in a parametric study taking the ML estimation as estimation procedure.

The ML estimator is that value of $\mathbf{a}$ which maximizes (15). Thus the ML estimator minimizes the quadratic form

$$Q(\mathbf{a}) = (\psi^m - \psi(\mathbf{a}))^T \mathbf{N}^{-1}(\psi^m - \psi(\mathbf{a})) \tag{85}$$

i.e., in the special case of a normal distribution the ML estimator and the least squares estimator with $\mathbf{N}^{-1}$ as weight matrix are identical.

The parametric study has been performed within the basic scenario of a stationary radar and a passive sensor flying a straight-line trajectory. In this case the sensor movement is within the plane defined by the initial LOS and the sensor velocity. Thus, the problem

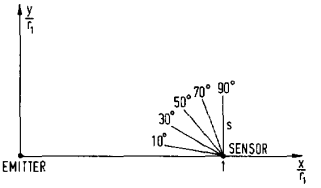

Fig. 9. Sensor trajectories considered in simulation; $r_1 = 10$ km, $s = 3$ km.

is two-dimensional and can be calculated in the system of coordinates of Fig. 2. For a constant r_1 and a fixed sensor path length s the trajectories merely differ in the aspect angle γ_1. In the simulation performed, the five angles $\gamma_1 = \{10°, 30°, 50°, 70°, 90°\}$ have been considered (Fig. 9). To determine the influence of the measurement error on the estimates, the standard deviations σ_B and σ_F have also been varied: $\sigma_B = \{5°, 10°\}$, $\sigma_F = \{50$ Hz, 100 Hz, 200 Hz$\}$. The other parameters have been fixed as follows:

initial radar sensor distance	$r_1 = 10$ km	
sensor path length	$s = 3$ km	
constant sensor velocity	$v = 300$ m/s	(86)
transmitter frequency	$\nu_0 = 3$ GHz	
sampling rate	$1/\Delta t = 10$ Hz.	

Some remarks concerning the parameter values are appropriate. To warrant the independence of individual measurements the sampling rate has not been chosen too high. Bearing measurement accuracies in the order of magnitude of 5 or 10 deg are no serious problem in practice. More serious are the high relative frequency accuracies in the case of pulsed signals. If the pulses are coherent, accuracies in the postulated range, however, can be attained [13].

Now, inserting the measurements into (85) and minimizing, the ML estimate of the radar position results. In Table I, II, and III the expected values of the estimation error are listed for BM, FM, and CM, respectively. In addition to that, the tables contain the corresponding error ellipses

$$(\mathbf{P}\widehat{\Delta\mathbf{a}})^T(\mathbf{P}\mathbf{C}\mathbf{P}^T)^{-1}\mathbf{P}\widehat{\Delta\mathbf{a}} = 1 \qquad (87)$$

where C denotes the covariance matrix of the estimation error.

The error ellipses are given in terms of the semiaxes e, f, and the angle of orientation β, i.e. the angle between the semimajor axis and the x-axis of the coordinate system. The expected values and semiaxes in the tables are given in meters, the angles in degrees, and the measurement errors σ_B and σ_F in degrees and Hertz, respectively. The results are the product of a Monte Carlo simulation of 6000 runs. In each run the quadratic form (85) has been minimized by applying the well-known iterative BFGS-procedure (see e.g., [14]).

TABLE I
Expectation and Error Ellipses of ML Estimation Error for BM as Function of σ_B and γ_1

σ_B	γ_1	$E[\Delta\hat{x}]$	$E[\Delta\hat{y}]$	β_B	e_B	f_B
	10		in 70 cases no convergence			
	30	−207	−21	5.7	1452	79
5	50	−104	−15	7.9	1046	82
	70	−88	−14	8.7	997	86
	90	−101	−16	8.3	1099	91
	10		in 352 cases no convergence			
	30*	−1057	−107	5.6	3997	184
10	50	−490	−68	7.9	2520	176
	70	−408	−64	8.7	2294	182
	90	−473	−72	8.4	2574	194

*Note:** No convergence in 22 cases.

TABLE II
Expectation and Error Ellipses of ML Estimation Error for FM as Function of σ_F and γ_1

σ_F	γ_1	$E[\Delta\hat{x}]$	$E[\Delta\hat{y}]$	β_F	e_F	f_F
	10		in 2045 cases no convergence			
	30*	−616	−1240	52	4575	1811
50	50	56	−344	56	1868	486
	70	279	−90	80	1418	428
	90	316	210	110	1575	521
	10		in 2048 cases no convergence			
	30		in 518 cases no convergence			
100	50	549	−1046	71	3180	1554
	70	910	−225	86	2303	1100
	90	1022	517	106	2486	1269
	10		in 1798 cases no convergence			
	30		in 1513 cases no convergence			
200	50	2218	−1672	85	4035	2883
	70	2277	−282	92	3055	2053
	90	2489	927	101	3206	2247

*Note:** No convergence in 40 cases.

From the above discussion of the estimation methods the accuracy of FM will decisively be dependent on the sensor dynamics. For the simple case of a nonmaneuvering sensor, mainly two factors have an influence on the estimation accuracy. First, the Doppler base, i.e., the Doppler variation along the sensor trajectory, and second, the distance from the sensor to the radar. In contrast to this the accuracy in BM depends on the radar sensor geometry only. Now, the angle base, i.e., the variation of the bearing angle along the sensor trajectory, and the distance to the radar determine the estimation accuracy. Generally, the larger the Doppler base or the larger the angle base and the smaller the distance, the better the estimation accuracy will be.

Of the cases considered $\gamma_1 = 70°$ is that with the largest Doppler and angle base. As can be seen from Tables I and II, the bias and error ellipses in this case are smallest. That is the integration gain from a larger base here proves to be more significant than the shorter radar sensor distance.

TABLE III
Expectation and Error Ellipses of ML Estimation Error for CM as Function of (σ_F, σ_P) and γ_1

$\frac{\sigma_F}{\sigma_P}$	γ_1	$E[\Delta\hat{x}]$	$E[\Delta\hat{y}]$	β_C	e_C	f_C
	10*	−824	1579	157	3032	2001
50	30	−14	−2.5	9.7	450	70
5	50	−2.1	−0.7	16	239	74
	70	−1.0	0.0	13	187	84
	90	−1.9	0.4	3.3	204	88
	10**	−2575	3283	25	4191	1934
50	30	−21	−13	16	596	108
10	50	0.6	−2.4	30	315	114
	70	2.1	0.1	41	213	149
	90	0.8	2.1	159	225	161
	10+	−1096	1658	174	3901	2178
100	30	−50	−5.6	6.7	752	76
5	50	−13	−2.0	9.9	421	80
	70	−8.1	−1.0	9.5	352	85
	90	−10	−0.9	7.0	385	90
	10	in 160 cases no convergence				
100	30	−72	−17	9.7	927	137
10	50	−13	−4.1	16	481	148
	70	−6.7	−1.2	13	375	169
	90	−9.5	0.5	3.3	410	177
	10	in 63 cases no convergence				
200	30	−114	−11	5.9	1115	78
5	50	−38	−5.2	8.3	685	81
	70	−27	−3.9	8.7	602	86
	90	−33	−4.2	7.9	660	90
	10	in 268 cases no convergence				
200	30++	−252	−33	6.6	1670	155
10	50	−61	−10	9.8	860	161
	70	−39	−5.9	9.4	715	172
	90	−47	−5.0	7.0	783	180

Note: No convergence in *5, **36, +34, and ++2 cases.

The Doppler and angle base also have an effect on the convergence behavior of the minimum search algorithm. For small γ_1 and thereby a small Doppler and angle base (see Fig. 9) the functional (85) may be so badly conditioned that the iterative procedure is not always convergent within a preset limit of 1000 iteration steps. In all cases where the algorithm failed in more than 1% of the sample size, values are omitted from the tables in order to avoid falsifications by a truncated statistic. In the other cases with convergence failure the values are based on the residual set of estimates.

As can be seen, in all cases the estimates in BM and FM have a significant bias violating in that way the presupposition of a biasfree estimate for the validity of the CR bound (30). Nevertheless, just like the CR bounds the ML error ellipses of BM and FM are clearly rotated with respect to each other, too.

From this we expect an integration gain that exceeds by far the statistical gain due to the additional measurements when applying CM. In fact, a comparison of Table III with Tables I and II shows

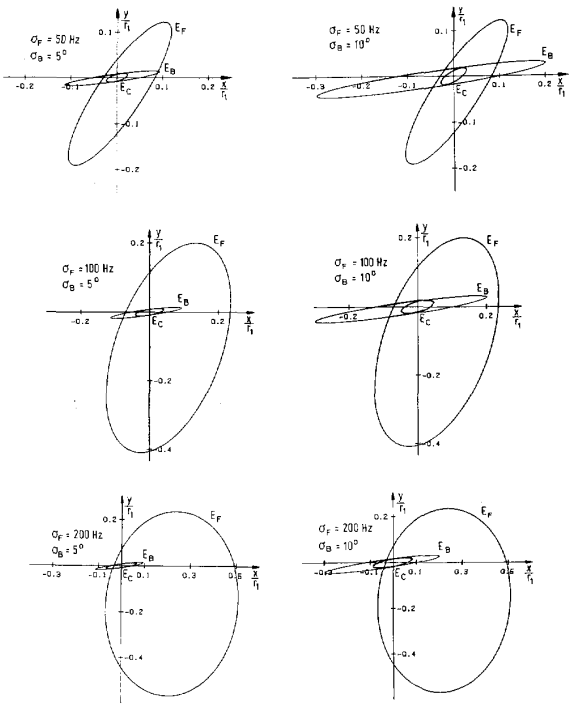

Fig. 10. ML error ellipses (87) for (86) and $\gamma_1 = 50°$.

that CM throughout leads to considerably smaller bias and error ellipses than BM and FM, respectively. Since CM is a combination of BM and FM, the estimation accuracy now is dependent on both the radar sensor geometry and the sensor dynamics. For a nonmaneuvering sensor that means the larger the Doppler and angle base and the smaller the radar sensor distance, the better the estimation accuracy will be.

Among the cases considered the highest estimation accuracy, therefore, is expected for $\gamma_1 = 70°$ again. In fact, in Table III bias and error ellipses are smallest for the case $\gamma_1 = 70°$ and the estimation errors increase with decreasing base and with increasing measurement error. At the same time we again observe a deterioration of the conditions for a successful minimum search, however, to an extent by far smaller than for BM and FM. So, CM is still converging in some cases where BM and FM already fail.

From Table III we conclude that in CM apart from the cases with extreme low Doppler and angle base ($\gamma_1 = 10°$) the ML estimate has no significant bias, this statement being violated the more the smaller the Doppler and angle base and the larger the measurement errors. The small bias justifies a comparison of the ML error ellipse with the CR bound (30). Calculations have shown that in all cases where the bias is small, the CR bound is a very good approximation to the ML error ellipse.

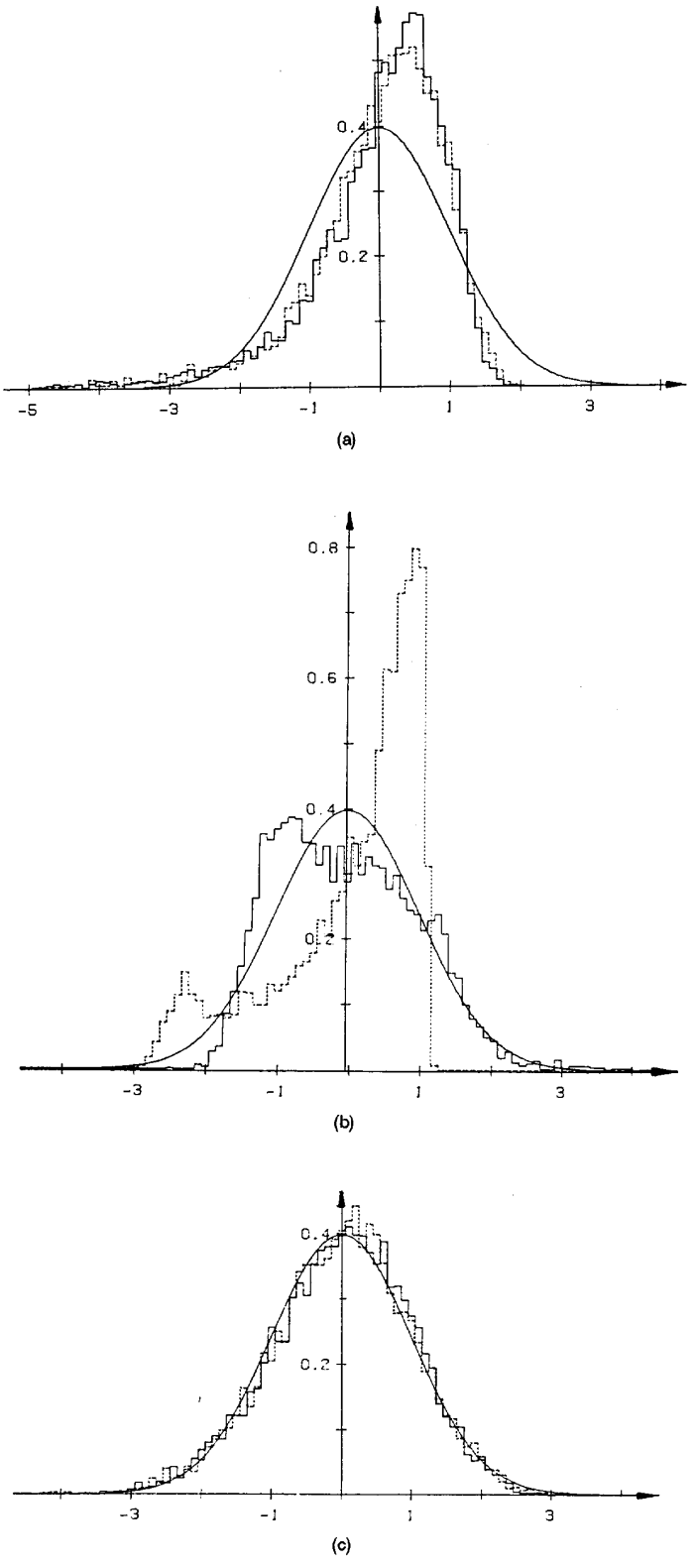

Fig. 11. Histogram of x-component (solid line) and y-component (dashed line) of standardized estimation error for (86), $\gamma_1 = 50°$, and (a) BM: $\sigma_B = 10°$; (b) FM: $\sigma_F = 100$ Hz, (c) CM: $(\sigma_F, \sigma_B) = (100$ Hz, $10°)$.

Fig. 10 illustrates for $\gamma_1 = 50°$ the gain in estimation accuracy by applying CM. For a better comparison with BM and FM in addition to the ML error ellipses E_C of CM the corresponding error ellipses E_B and E_F of BM and FM have been depicted. Also contained in the figures are the CR bounds of CM. They practically coincide with E_C. For a comparison of the error ellipses note the different scale for different σ_F. As can be seen, from the different orientation of E_B and E_F a considerable improvement of the estimation accuracy results. The estimate is practically biasfree. Moreover, by a comparison of E_C with the CR bound the near optimality of the estimate clearly comes to light.

Apart from the strongly improved estimation accuracy the ML estimate of CM also distinguishes itself from those of BM and FM by its distribution. For measurement errors in the range considered in this study the position estimate proved to be quasi-normally distributed. The same does not hold true in case of BM and FM. This fact is well reflected by the marginal distributions of the position coordinates which have to be normally distributed in case of a jointly normal position estimate. As an illustration let us consider the case $\gamma_1 = 50°$ with $\sigma_F = 100$ Hz and $\sigma_B = 10°$. For CM the distributions depicted in Fig. 11(c) result. The figure shows the histograms of the x-component and the y-component of the standardized estimation error. From a comparison with the density function of the normal distribution with zero mean and variance $\sigma^2 = 1$, also plotted in the figure, one can see that the marginal distributions of the estimation error only insignificantly differ from the normal distribution. Quite different, however, it is with BM and FM. Now, for the same measurement errors the histograms significantly deviate from the normal distribution (Fig. 11(a), (b)).

The quasi-normal distribution of the estimates in CM has an important practical meaning. It allows for an interpretation of the error ellipses as ellipses of definite probability whereas in BM and FM they are only a rough measure of the spread of errors.

V. SUMMARY AND CONCLUSIONS

In this study we have considered the problem of locating a stationary emitter from passive bearing and frequency measurements taken by a moving and autonomously operating sensor along its trajectory. The estimation procedure based on bearings only is quite different from that based on frequency measurements. From the CR analysis of the single measurement case the characteristic features of each method become transparent and an intuitive understanding of both methods is provided. One of the major results is that the orientation of the error ellipses of BM and FM significantly differ. From this a considerable integration gain in accuracy results, when processing the combined set of bearing and frequency measurements.

The results of the theoretical CR analysis are verified very well in a numerical simulation based on the ML estimation procedure. The simulations demonstrate that CM is definitely superior to BM and FM with respect to the bias and the size of the error ellipses just as well. This is mainly due to the different orientation of the error ellipses of BM and FM, respectively. As opposed to BM and FM, the estimation in CM is nearly biasfree even for medium measurement errors. In this case the CR bound proved to be a very good approximation to the ML error ellipses. So, in the range of measurement errors considered, time-consuming simulations can be avoided by performing less extensive CR calculations. At the same time the quasi-normal distributions allow for an interpretation of the error ellipses as ellipses of definite probability.

In the investigations performed we have not optimized the trajectories in order to minimize the location accuracy. Whereas in BM only the emitter sensor geometry enters into the estimation problem, in FM and thereby in CM, the sensor dynamics also will have a strong impact on the estimation accuracy. A steerable sensor, when locating an emitter, may take advantage of that fact.

REFERENCES

[1] Stansfield, R. G. (1947)
Statistical theory of DF fixing.
Journal of the IEE, **94**, 15 (1947), 762–770.

[2] Foy, W. H. (1976)
Position-location solutions by Taylor series estimation.
IEEE Transactions on Aerospace and Electronic Systems, **AES-12** (Mar. 1976), 187–194.

[3] Torrieri, D. J. (1984)
Statistical theory of passive location systems.
IEEE Transactions on Aerospace and Electronic Systems, **AES-20** (Mar. 1984), 183–198.

[4] Van Keuk, G. (1978)
Extended Kalman filter for triangulation in a variable multi-sensor-system.
Regelungstechnik, **10** (1978), 331–336.

[5] Spingarn, K. (1987)
Passive position location estimation using the extended Kalman filter.
IEEE Transactions on Aerospace and Electronic Systems, **AES-23** (July 1987), 558–567.

[6] Ancker, C. J. (1958)
Airborne direction finding—The theory of navigation errors.
IRE Transaction on Aeronautical and Navigational Electronics, **ANE-5** (Dec. 1958), 199–210.

[7] Wax, M. (1983)
Position location from sensors with position uncertainty.
IEEE Transactions on Aerospace and Electronic Systems, **AES-19** (Sept. 1983), 658–662.

[8] Poirot, J. L., and McWilliams, G. V. (1974)
Application of linear statistical models to radar location techniques.
IEEE Transactions on Aerospace and Electronic Systems, **AES-10** (Nov. 1974), 830–834.

[9] Poirot, J. L., and Arbid, G. (1978)
Position location: Triangulation versus circulation.
IEEE Transactions on Aerospace and Electronic Systems, **AES-14** (Jan. 1978), 48–53.

[10] Mangel, M. (1981)
Three bearing method for passive triangulation in systems with unknown deterministic biases.
IEEE Transactions on Aerospace and Electronic Systems, **AES-17** (Nov. 1981), 814–819.

[11] Levanon, N., and Ben-Zaken, M. (1985)
Random error in ARGOS and SARSAT satellite positioning systems.
IEEE Transactions on Aerospace and Electronic Systems, **AES-21** (Nov. 1985), 783–790.

[12] Van Trees, H. L. (1968)
Detection, Estimation, and Modulation Theory, Part I.
New York: Wiley, 1968.

[13] Becker, K. (1990)
New algorithm for frequency estimation from short coherent pulses of a sinusoidal signal.
IEE Proceedings, **137**, Pt. F (Aug. 1990), 283–288.

[14] Broyden, C. G. (1970)
The convergence of a class of double rank minimization algorithms 2. The new algorithm.
Journal of the Institute of Mathematics and Its Applications, **6** (1970), 222–231.

Klaus Becker was born in 1944 in Olpe, Germany. He received the degree of a Dipl. Phys. and the Dr. degree in physics from the University of Mainz in 1973 and the University of Bonn in 1976, respectively.

In 1976 he entered the Research Institute for Electronics and Mathematics (FFM) in Wachtberg-Werthhoven, Germany, where he has been working in the field of sensor data processing. His principal research interests are in automatic control, tracking systems, and position-location techniques.